Inhibition of glioblastoma progression by Urolithin A *in vitro* and *in vivo* by regulating Sirt1-FOXO1 axis via ERK/AKT signaling pathways

Cui-Lan LIU[1,2,#,*], Di ZHAO[1,2,#], Jian-Jun LI[3], Song LIU[4], Jia-Jia AN[5], Dan WANG[1,2], Feng-Ai HU[1,2], Chang-Yun QIU[1,2], Ming-Hu CUI[2,*]

[1]Institute for Metabolic and Neuropsychiatric Disorders, Binzhou Medical University Hospital, Binzhou, Shandong, China; [2]Department of Psychology, Binzhou Medical University Hospital, Binzhou, Shandong, China; [3]Emergency Department, First People's Hospital of Jinan, Jinan, Shandong, China; [4]Thyroid and Breast Surgery Department, Binzhou Medical University Hospital, Binzhou, Shandong, China; [5]Department of Clinical Laboratory, Binzhou Medical University Hospital, Binzhou, Shandong, China

*Correspondence: chouzi_19@163.com
#Contributed equally to this work.

Glioblastoma (GBM) is the most universal and devastating primary intracranial neoplasm in the central nervous system. Urolithin A (UA) possesses many pharmacological and biological activities, but its function in GBM is not clear. CCK-8 and colony formation test were used to measure the anti-proliferative potency of UA against GBM cells. Flow cytometry was applied to evaluate cell cycle arrest and apoptosis of U251 and U118 MG cells upon UA incubation. Quantitative real-time PCR and western blotting were conducted to test the regulatory effect of UA on the expression of Sirt1 and FOXO1. Immunodeficient mice were implanted with GBM cells for *in vivo* validation of the anti-cancer effect of UA. We found UA repressed the proliferation, migration and invasion of glioblastoma cells, while also inhibiting the induction of colony formation ability and epithelial to mesenchymal transition (EMT) in a time- or dose-dependent manner. The does-dependent relationship of UA inducing the cell cycle arrest and apoptosis of glioblastoma cells was identified. Furthermore, UA could enhance the expression levels of Sirt1 and FOXO1 and the knockdown of Sirt1 blocked the inhibitory effects of UA on the proliferation and migration of glioblastoma cells and correspondingly modified the expression level of FOXO1. Overexpression of Sirt1 restored the despaired inhibitory effect of UA induced by Sirt1 knockout on the proliferation and migration of glioblastoma cells. In animal experiments, UA decreased the tumor size and weight of glioblastoma in xenograft nude mice and promoted the expression of Sirt1 and FOXO1 in transplanted tumors. Our findings presented in this study indicate that UA exerts a repressive effect on glioblastoma cells *in vivo* and *in vitro* by regulating the Sirt1-FOXO1 axis via the ERK and AKT pathways, indicating that UA is a new novel therapeutic candidate for the treatment of glioblastoma.

Key words: glioblastoma, Urolithin A, proliferation, Sirt1, FOXO1

Glioblastoma (GBM) is the most universal and devastating primary malignant tumor in the central nervous system, characterized by rapid growth, strong aggressiveness, and extensive infiltration in adjacent brain areas [1, 2]. Although surgery combined with chemotherapy and radiotherapy can extend survival to some extent, the median survival time of GBM patients remains poor (14 months after diagnosis) [3]. As a result, the mortality rate of GBM is extremely high [4]. Therefore, the development of therapeutic strategies that can extend the survival time of GBM patients and improve their living quality is imperative, especially drugs that can penetrate the blood-brain barrier (BBB) [5].

At present, natural compounds have attracted increasing attention because of their low cost, high bioavailability, and limited toxicity, possessing intrinsic antioxidant, anti-inflammatory, and antitumor activities. Urolithins, including urolithin A (UA), urolithin B (UB), urolithin C (UC), and urolithin D (UD), are the intestinal microbial metabolic products of both ellagitannins and ellagic acid [6]. Ellagitannins (ETs) consist of a variety of hydrolyzable tannins and can be hydrolyzed to produce ellagic acid (EA) in the gut, and ETs are mainly present in fruits, such as pomegranates, blackberries, and strawberries [7]. Recently, the biological functions of urolithins have been studied *in vitro* and *in vivo*, including anti-inflammation activity, anti-proliferation in cancer, antioxidant activity, and beneficial effects on lipid metabolism and prolonged lifespan [8, 9]. Among the different urolithins, UA exhibits potent antioxidant and anti-inflammatory properties, indicating it may be the dominant compound responsible for the intrinsic antitumor activity of EA [10–12]. However, the effect of UA in glioblastoma has not yet been investigated.

Sirt1, a mammalian homolog of silent information regulator 2 (Sir2), is the founding member of the sirtuin family [13]. The NAD(+)-dependent class III histone deacetylase Sirt1 is highly conserved across species, which deacetylates histones and affects gene expression epigenetically [14, 15], as well as modulating the functions of specific transcription factors and enzymes/proteins by regulating the acetylation [16]. Sirt1 has shown promising associations with protein deacetylation and is involved in numerous biological or pathological processes, such as energy metabolism, autophagy, aging, and inflammation [17, 18], especially its role in cancer [19]. FOXO1, also known as FKHR, is one member of the FOXO transcription factors family, which commonly has a conserved winged-helix DNA-binding domain [20]. FOXO proteins play important roles in the regulation of gene transcription by binding to the functional sequence of target genes. Increasing evidence has shown that the FOXO1 expression levels are decreased in some types of cancer with poor outcomes [21]. Moreover, FOXO1 proteins are usually amassed in the nucleus and serve as transcriptional regulators in non-tumor tissues. The tumor suppressor gene FOXO1 can inhibit tumor growth. Previous researches have shown that FOXO1 inhibits proliferation, prevents invasion, and induces apoptosis in gliomas [22].

In this study, we investigated the inhibitory effects of UA on glioblastoma cell growth, migration, invasion, and EMT *in vitro*, and tumor growth *in vivo*. We then tested its regulatory ability on apoptosis and the cell cycle. Furthermore, we assessed whether the expression of Sirt1 and FOXO1 could be regulated by UA and determined whether UA is a potential therapeutic drug candidate for glioblastoma treatment.

Materials and methods

Cell culture and drugs. The human glioblastoma cell lines U251, U118 MG, and U87 MG were obtained from the American Type Culture Collection (ATCC) (ATCC, Manassas, VA, USA). Normal human astrocyte (NHA) cells (catalog #1800) were purchased from ScienCell Research Laboratories (Carlsbad, CA, USA). Cell lines were cultured in Dulbecco's minimal essential medium or astrocyte medium (AM, #1801) supplemented with 10% fetal bovine serum at 37 °C in a 5% CO_2 humidified incubator. The stock solution (100 mM) of Urolithin A (UA) (#SML1791; Sigma-Aldrich, St. Louis, MO, USA) was prepared by dissolving in dimethyl sulfoxide.

Knockdown of Sirt1 and overexpression of Sirt1 and FOXO1 genes and plasmid transfection. To construct the Sirt1 short hairpin RNA plasmid, the oligonucleotides TTGGATGATATGACACTG were cloned into the pGPU6/Neo vector. The pGPU6/Neo-GFP scramble oligonucleotides vector (Genepharma, Shanghai, China) was used as the control. The Sirt1 and FOXO1 overexpression plasmids were purchased from Wuhan Yipu Biological Technology Co. Ltd. (Wuhan, China). The nucleotide sequences of all the vectors were verified by DNA sequencing. Transfection of glioblastoma cells was performed using Lipofectamine 3000 (Invitrogen, Carlsbad, CA, USA). The transfection efficiencies of the shRNA plasmids were determined by fluorescence microscopy (Zeiss Axio Imager Z1 Fluorescent Microscope).

Western blotting analysis. The separation of the mitochondria fractions was conducted using the Cell Mitochondria Isolation Kit (C3601; Beyotime Biotechnology, Shanghai, China) according to the manufacturers' instructions. Western blotting was performed as described previously [23–25]. Briefly, cells were lysed in RIPA lysis buffer (Beyotime Biotechnology). BCA protein assay kit (Vazyme, Nanjing, China) was used to determine the protein concentrations. The protein mixtures were separated by 12% or 15% SDS-PAGE gel and transferred to a polyvinylidene fluoride membrane (Millipore, Billerica, MA, USA) in a Trans-Blot SD semidry transfer cell (Bio-Rad, Hercules, CA, USA). The membranes were blocked by 5% non-fat powdered milk in TBST buffer at pH 7.4 (20 mM Tris–HCl, 150 mM NaCl, 0.1% Tween-20) and then probed with Anti-Cytochrome C (1:1000, #4272; Cell Signaling Technology, Danvers, MA, USA), VDAC1/2 (1:1000) (10866-1-AP; Proteintech, Wuhan, China), Anti-Bcl-2 (1:200, #15071; Cell Signaling Technology), Anti-Bax (1:200, #5023; Cell Signaling Technology), Anti-CDK4 (1:1000, #12790; Cell Signaling Technology), Anti-Cyclin D1 (1:1000, #2922; Cell Signaling Technology), Anti-Vimentin (1:1000, #YM6529; Immunoway), anti-E-cadherin (1:5000, #20874-1-AP; Proteintech), Sirt1 antibody (1:1000, #07-131; Sigma-Aldrich), Anti-FOXO1 (1:1000, #2880; Cell Signaling Technology), Anti-p-p38 (1:1000, #9215; Cell Signaling Technology), Anti-p38 (1:1000, #9212; Cell Signaling Technology), Anti-p-JNK (1:1000, #9251; Cell Signaling Technology), Anti-JNK (1:1000, #9252; Cell Signaling Technology), Anti-AKT (1:1000, #4691; Cell Signaling Technology), Anti-p-AKT (Thr308) (1:1000, #2965; Cell Signaling Technology), and Anti-β-actin (1:1000, #4970; Cell Signaling Technology) antibodies at 4 °C overnight. After washing, the membranes were incubated with goat anti-rabbit IR Dye 680LT (1:5000, #926-68021; Li-COR Biosciences, Lincoln, NE, USA) or goat anti-mouse IR Dye 800CW (1:5000, #926-32210; Li-COR Biosciences) fluorescent secondary antibodies and visualized with Odyssey infrared imaging system (Li-COR Biosciences).

Quantitative real-time PCR. Total RNA was extracted by using Total RNA Kit (#R6834; OMEGA Bio-teck, Doraville, GA, USA) and purified according to the manufacturer's recommendations. Following, reverse transcription was performed using 5× HiScript II QRT SuperMix (Vazyme). The cDNA was detected by the StepOnePlus real-time PCR system (Applied Biosystems, Waltham, MA, USA) with AceQ qPCR SYBR Green Master Mix (Vazyme) according to the operating instructions. The following primer sequences were used to amplify each product: Cyclin D1 forward: 5'-GCTGCGAAGTGGAAACCATC-3' and reverse: 5'-CCTCCTTCTGCACACATTTGAA-3'; CDK4 forward: 5'-ATGGCTACCTCTCGATATGAGC-3' and reverse:

5'-CATTGGGGACTCTCACACTCT-3'; Sirt1 forward: 5'-TAGCCTTGTCAGATAAGGAAGGA-3' and reverse: 5'-ACAGCTTCACAGTCAATTTGT-3'; FOXO1 forward: 5'-TCGTCATAATCTGTCCCTACACA-3' and reverse: 5'-CGGCTTCGGCTCTTAGCAAA-3'; GAPDH forward: 5'-AGAAGGCTGGGGCTCATTTG-3', and reverse: 5'-AGGGGCCATCCACAGTCTTC-3'. The $2^{-\Delta\Delta CT}$ method was used to calculate the relative fold-change of gene expression levels normalized to the housekeeping gene GAPDH compared with the control samples [26, 27].

Immunofluorescence staining. Cells or tumor tissues were fixed with 4% paraformaldehyde. Then the tumor tissues were moved to 30% sucrose and cut into 20 μm coronal sections. The cells or slices were permeabilized with 0.5% Triton X-100 for 20 min, and blocked with 10% horse serum for 30 min, and incubated for 1 h with Ki67 antibody (1:200, #ab16667; Abcam, Cambridge, UK), FOXO1 antibody (1:250, #2880; Cell Signaling Technology), or Sirt1 antibody (1:250, #07-131; Sigma-Aldrich) at room temperature. Then the sections were washed with PBS and incubated with donkey anti-rabbit 546 (1:400, #A21206; Invitrogen, Carlsbad, CA, USA) for 1 h at room temperature. After washing with PBS, the sections were incubated with DAPI (3 μg/ml) (Beyotime Biotechnology) for 5 min to stain nuclei. Lastly, the stained sections were washed three times with PBS and put on poly-lysine-coated glass slides with coverslips, and captured using confocal microscopy (Olympus, Tokyo, Japan) under identical conditions.

For Ki67-positive cell quantification, eight random regions of each slice were selected; the cell number of each region was counted by experimenters who were blind to the treatment manually. For Sirt1 and FOXO1 immunofluorescence signal intensity semi-quantification, the immunofluorescence images were converted to grayscale, eight random regions of each slice were selected (10 slices/mice), and the signal intensity of immunolabelling in each region was quantified as integrated density using the ImageJ software (http://imagej.nih.gov/ij/) as described previously [23]. The average gray values were calculated as: [integrated density-(measured area×mean background signal)]/measured area. The areas without signal were taken as a background signal. The density of each tissue sections was averaged and shown as a percentage relative to the control.

Cell proliferation assay. Cells were counted and inoculated at a density of 3,000 cells/well in 96-well plates. Multiple concentrations of UA were administered to cells, and the CCK-8 assay (MCE, New Jersey, USA) was performed at 24 h, 48 h, and 72 h, according to the manufacturer's protocol [28]. The absorption was measured with a microplate reader (SpectraMax M5; Molecular Devices, CA, USA) at 450 nm. The relative absorption was normalized to the control. Experiments were performed in triplicates.

Colony formation assay. Cells were cultured in 12-well plates and treated with various concentrations of UA for 48 h. Then, the cells were cultured for another 14 days with a medium without UA. The cells were fixed with methanol and stained with 0.1% crystal violet solution for 20 min. The numbers of colonies were counted. Experiments were performed in triplicates.

Wound-healing assay. To assess the cell migration and cell interactions, a wound-healing assay was conducted and analyzed, as described previously [28]. About 1×10^6 cells/well were inoculated into 6-well plates. 24 h later, the cells were scraped using a 200 μl tip and incubated with serum-free medium containing multiple concentrations of UA for 24 h or 48 h. Photomicrographs were taken before and after treatment using optical microscopy (IX53; Olympus). The relative distances of the wound width before treatment minus the wound width after treatment were calculated and quantified using ImageJ software. Experiments were performed in triplicates.

Transwell assay. The cells were seeded into 150 μl serum-free DMEM medium in the upper chamber with Transwell inserts (8 μm pore size) (Corning, NY, USA) coated with or without matrigel. Then, 20% FBS DMEM was added to the lower chamber. The top chambers contained different concentrations of UA. After 24 h, the cells located on the upper surface of the membrane were removed and the wells were stained with 0.1% crystal violet solution for 20 min (#E607309; Sangon Biotech Co., Ltd., Shanghai, China), washed with PBS, and then photographed with light microscopy (IX53; Olympus). Three random fields were selected for cell number counting. Experiments were performed in triplicates.

Apoptosis and cell cycle analysis. The procedure of the apoptosis and cell cycle analysis was conducted as described previously [28, 29]. For the apoptotic cell test, the cells were treated with several different concentrations of UA for 24 h, then washed using ice-cold PBS, and stained with Annexin V-FITC mixture for 15 min at 4°C, then stained with propidium iodide (PI) 5 min before detection using the FITC Annexin V Apoptosis Detection Kit according to the manufacturer's instructions (#556547; BD Biosciences, Franklin Lakes, NJ, USA). For the cell cycle test, the cells were incubated with diverse concentrations of UA for 24 h, washed with PBS, fixed with ice-cold 70% ethanol at 4°C overnight, and dyed with PI/RNase staining buffer for 15 min away from light, according to the manufacturer's instructions (#550825; BD Biosciences). After full resuspension, the CFlow Plus package from Accuri C6 was used to detect fluorescent signals. The dots in the left lower quadrant represent viable cells, while dots in the right lower and upper quadrants indicate early and terminal apoptotic cells. Experiments were performed in triplicates.

Animal studies. Male nude mice (BALB/c nu/nu, 4 weeks old, 13–14 g) were obtained from Jinan Pengyue Experimental Animal Breeding Co. Ltd. (Jinan, Shandong, China). The mice were provided with sterilized food and water *ad libitum* and were acclimatized for 7 days before the experiments [30]. Briefly, subcutaneous tumors were established by inocu-

lating 1×10^7 U251 cells near the axillary fossa of nude mice. Mice injected with tumor cells were divided into a vehicle or UA (50 mg/kg) dissolved in 0.5% carboxymethylcellulose treated groups (7 mice/group) randomly. All treatments were administered intragastrically on a daily basis. Tumor volumes were measured every 2 days using a caliper and calculated according to the formula V=1/2(width²×length). After gavage with UA or vehicle for 15 days, all the mice were anesthetized with ether and sacrificed, and the tumor weight of each mouse was measured. All animal experiments were approved by the Institutional Animal Care and Use Committee of Binzhou Medical University Hospital in accordance with the National Institutes of Health Guide for the Care and Use of Laboratory Animals (NIH Publications No. 8023, revised 1978).

Statistical analysis. The statistical software GraphPad Prism 8 was used to perform all statistical analyses. The normality and equal variance assumptions were performed using Shapiro-Wilk test and F test, respectively. For analysis of three or more groups, one-way analyses of variance (ANOVA) with Sidak post-hoc tests were applied. The linear relationships between two variables were evaluated by calculating Pearson's correlation coefficient. The value of $p<0.05$ indicated that there was a statistical significance. All data are presented as mean ± standard error (SEM).

Results
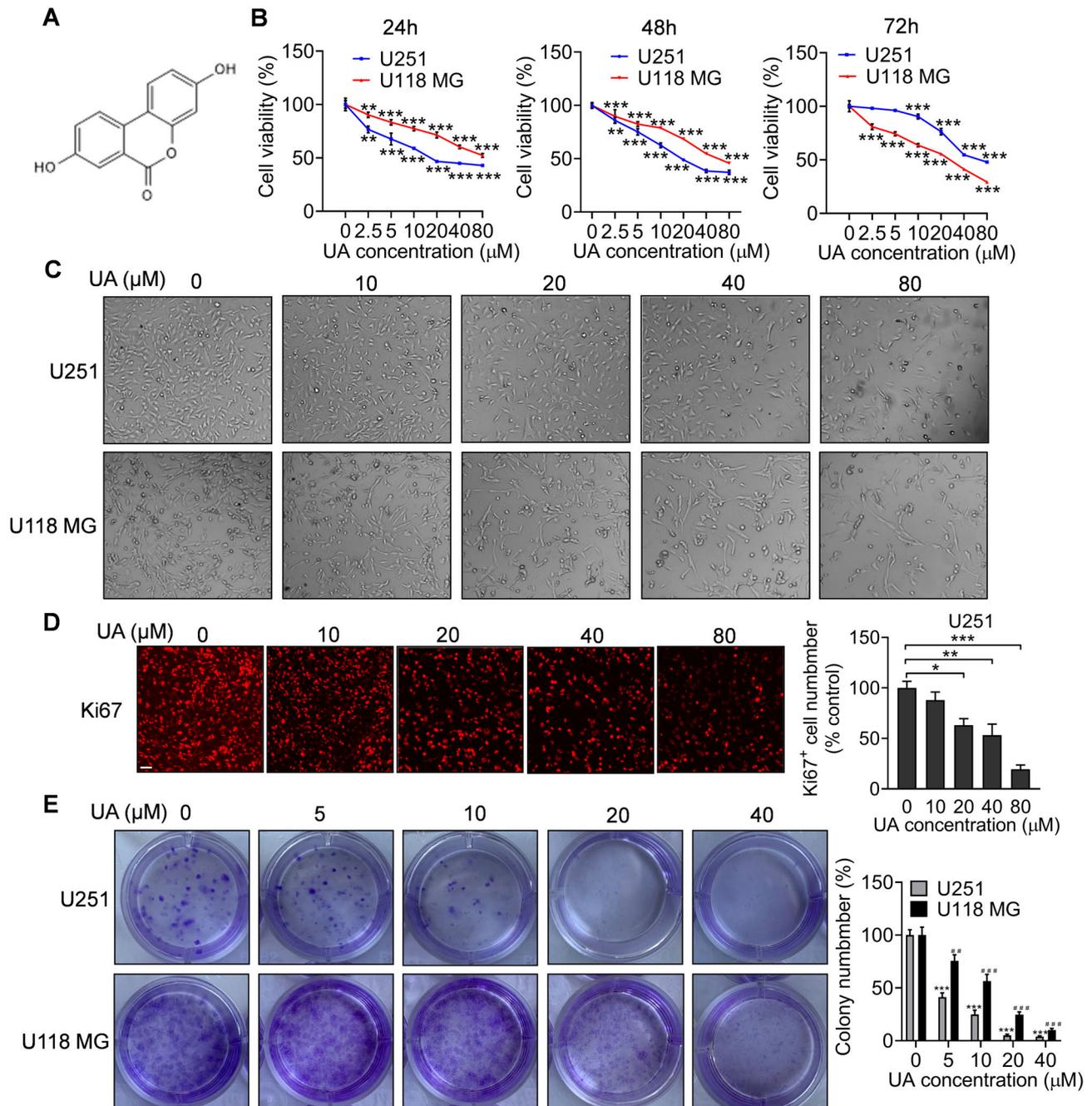
UA suppresses the growth of U251 and U118 MG cells. To investigate the inhibitory effects of UA on glioblastoma cells, the effects of a series of concentrations of UA on cell proliferation were examined in U251 and U118 MG cell lines at 24 h, 48 h, and 72 h (Figure 1A). We found that UA markedly suppressed the proliferation of U251 and U118 MG cells at 24 h, 48 h, and 72 h in a time- and/or dose-dependent manner, except for the two low concentrations (2.5 and 5 µmol/l) on U251 cells at 72 h (Figure 1B). The IC_{50} values of UA for inhibiting cell viability in the two cell lines were 9.33 µmol/l (U251) and 28.42 µmol/l (U118 MG) at 48 h, respectively. As shown in Figure 1C, UA decreased the contact among cells, and compared with the control group, the treated cells showed decreased spreading and formation of filopodia in a dose-dependent manner. Furthermore, our immunofluorescence staining of the proliferation marker Ki67 protein showed that UA significantly reduced the levels of Ki67-expressing in a dose-dependent relationship compared to the control group (Figure 1D). The colony formation experiment was assayed to test the effect of UA on the ability of colony-forming of U251 and U118 MG cells, and we found that UA significantly decreased the number of colonies in a dose-dependent manner (Figure 1E).

UA inhibits the migration and invasion of U251 and U118 MG cells. The effect of UA on the migratory activity of GBM cells was observed by wound-healing assay. The results showed that the migration of U251 cells was power-

fully inhibited by 10 µM UA at 24 h, while it was sensitive to the dose of UA at 5 µM at 48 h (Figure 2A, Supplementary Figure S1). Meanwhile, UA at 5 µM markedly suppressed cell migration of U118 MG cells at both 24 h and 48 h (Figure 2A, Supplementary Figure S1). By the way, the migratory growth and invasive expansion of U251 and U118 MG cells exposed to UA at different concentrations for 24 h were dramatically reduced in the Transwell assay (Figures 2B, 2C). Furthermore, to identify the role of UA in EMT, we evaluated the variations in E-cadherin and vimentin levels associated with UA treatment. Western blotting results showed that UA decreased the protein level of vimentin, and increased that of E-cadherin in U251 cells (Figure 2D).

UA induces cell cycle arrest and apoptosis of U251 and U118 MG cells. Cell proliferation is associated with cell cycle arrest. Thus, we evaluated the effect of UA on cell cycle arrest. The results showed that a large proportion of UA-treated cells showed dose-dependent growth arrest at the G2/M phase. The percentage of cells in the G2/M phase increased from 17.21±1.09% to 54.23±0.85% in U251 and from 4.97±0.47% to 53.69±1.77% in U118 MG. In contrast, the proportion of cells in the G0/G1 phase decreased from 53.76±4.51% to 12.41±0.66% in U251, and from 68.90±0.90% to 34.30±1.55% in U118 MG (Figure 3A, Supplementary Figure S2A). Furthermore, after treatment with UA for 48 h, we examined the mRNA and protein expression levels of the cell cycle-related proteins Cyclin D1 and CDK4 in U251 cells and found that UA markedly reduced the mRNA and protein levels in a concentration-dependent manner (Figures 3B, 3C). Apoptosis is a mechanism of cell suicide and a key mechanism underlying anticancer therapy [31]. Thus, we tested whether UA-induced cell growth inhibition was related to increased apoptosis of neuroblastoma cells. We found that UA treatment resulted in significant induction of apoptosis of U251 and U118 MG cells in a dose-dependent manner (Figure 3D, Supplementary Figure S2B). The release of Cytochrome C from mitochondria to the cytoplasm is an important step to activate cell apoptosis [32]. Western blotting results showed that the expression of Cytochrome C in the total cellular contents of U251 cells was increased with the increase of UA concentration (Figures 3E, 3F). As it was noted that Cytochrome C was released from mitochondria [33], therefore, the concentrations of Cytochrome C in mitochondria and cytoplasm were detected respectively, and we found that the protein levels of Cytochrome C in mitochondria was decreased, and increased in the cytoplasm by UA treatment (Figure 3G). For further confirmation, western blotting analysis was used to evaluate the expression of two key pro-apoptotic proteins, Bax and Bcl-2. Treatment with UA was found to significantly increase the expression of Bax and decrease the levels of Bcl-2 protein (Figures 3E, 3F).

The pivotal role of the Sirt1-FOXO1 pathway in the UA-mediated inhibition of glioblastoma cell growth and migration. To evaluate the relationship between the expression levels of Sirt1 and patient survival, we analyzed

Figure 1. UA repressed the growth of U251 and U118 MG cells. A) Chemical structure of UA. B) CCK-8 assay showing that UA inhibited U251 and U118 MG cell proliferation in a dose- and time-dependent manner. C) The morphology and proliferation changes of U251 and U118 MG cells after UA treatment for 48 h. (original magnification, 40×). D) Immunofluorescence image showing Ki67-expressing cells after UA incubation. Scale bar=50 μm. E) Western blotting indicating the protein expression levels of Ki67 in U251 cells after UA incubation. n=6; *p<0.05, **p<0.01, ***p<0.001 vs. vehicle-treated group

the Chinese Glioma Genome Atlas (CGGA; http://www.cgga.org.cn/) database. As a result, patients with higher Sirt1 expression had higher rates of survival (Figure 4A). The analysis of Sirt1 expression in different World Health Organization (WHO) grades indicated that the mRNA levels of Sirt1 in glioblastomas of WHO grade III and IV were significantly lower than in WHO grade II glioblastomas, indicating that the decrease of Sirt1 was associated with increased severity of glioblastoma (Figure 4B). To further evaluate the expression of Sirt1 in glioblastoma cell

lines, we quantitatively examined the mRNA levels of Sirt1 in three human glioblastoma cell lines. The results showed that the Sirt1 mRNA levels of glioblastoma cell lines were decreased compared to that of the control normal human astrocytes (Figure 4C). Next, we determined whether the

expression of Sirt1 was affected by UA, and found that the mRNA and protein levels of Sirt1 in U251 cells increased with the increase of the concentration of UA (Figures 4D, 4E), and accompanied by an increase of the mRNA and protein levels of FOXO1 (Figure 4F, 4G). The correlation
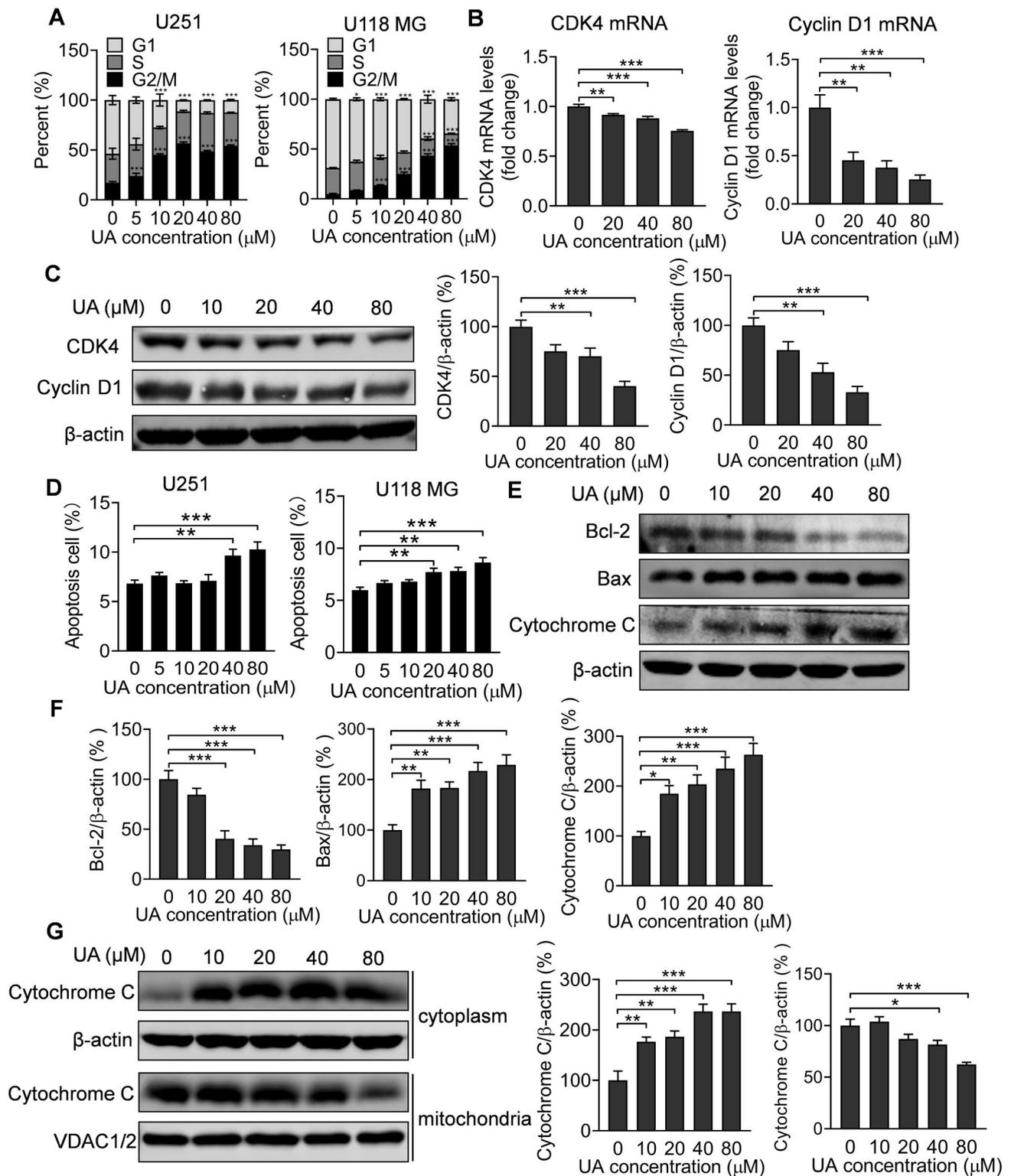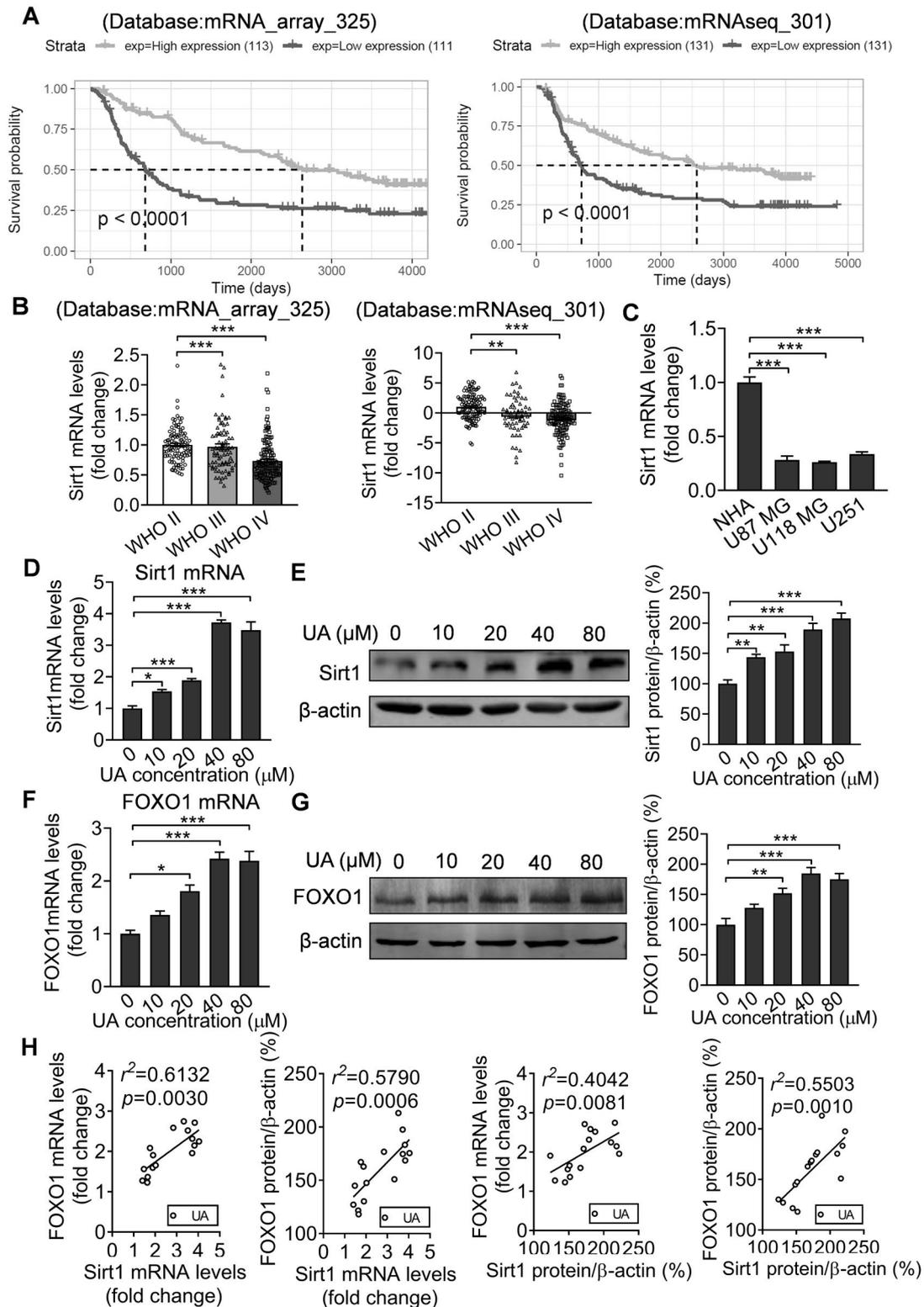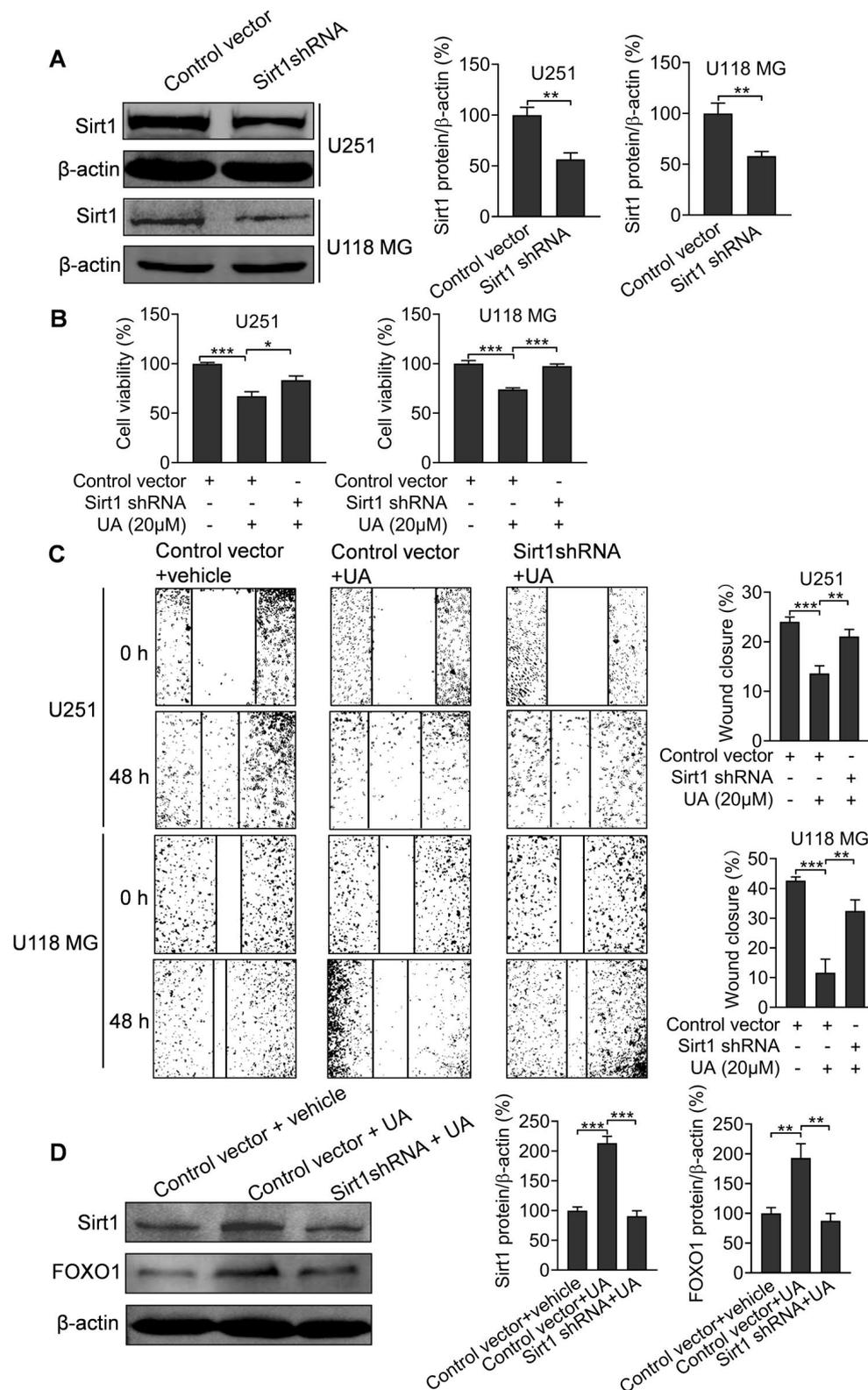

Figure 2. Inhibition of migration, invasion, and EMT by UA of U251 and U118 MG cells. A) Quantified analysis of the wound-healing assay results indicated that UA suppressed the migration ability of U251 and U118 MG cells at 24 h and 48 h in a dose-dependent manner. B) Transwell assay showed that UA inhibited migratory capability of U251 and U118 MG cells. (Original magnification, 40×). C) The inhibitory activity of UA on invasion was detected by Transwell assays. D) The EMT-associated protein Vimentin and E-cadherin was assessed by western blotting. n=6; *p<0.05, **p<0.01, ***p<0.01 vs. vehicle-treated group
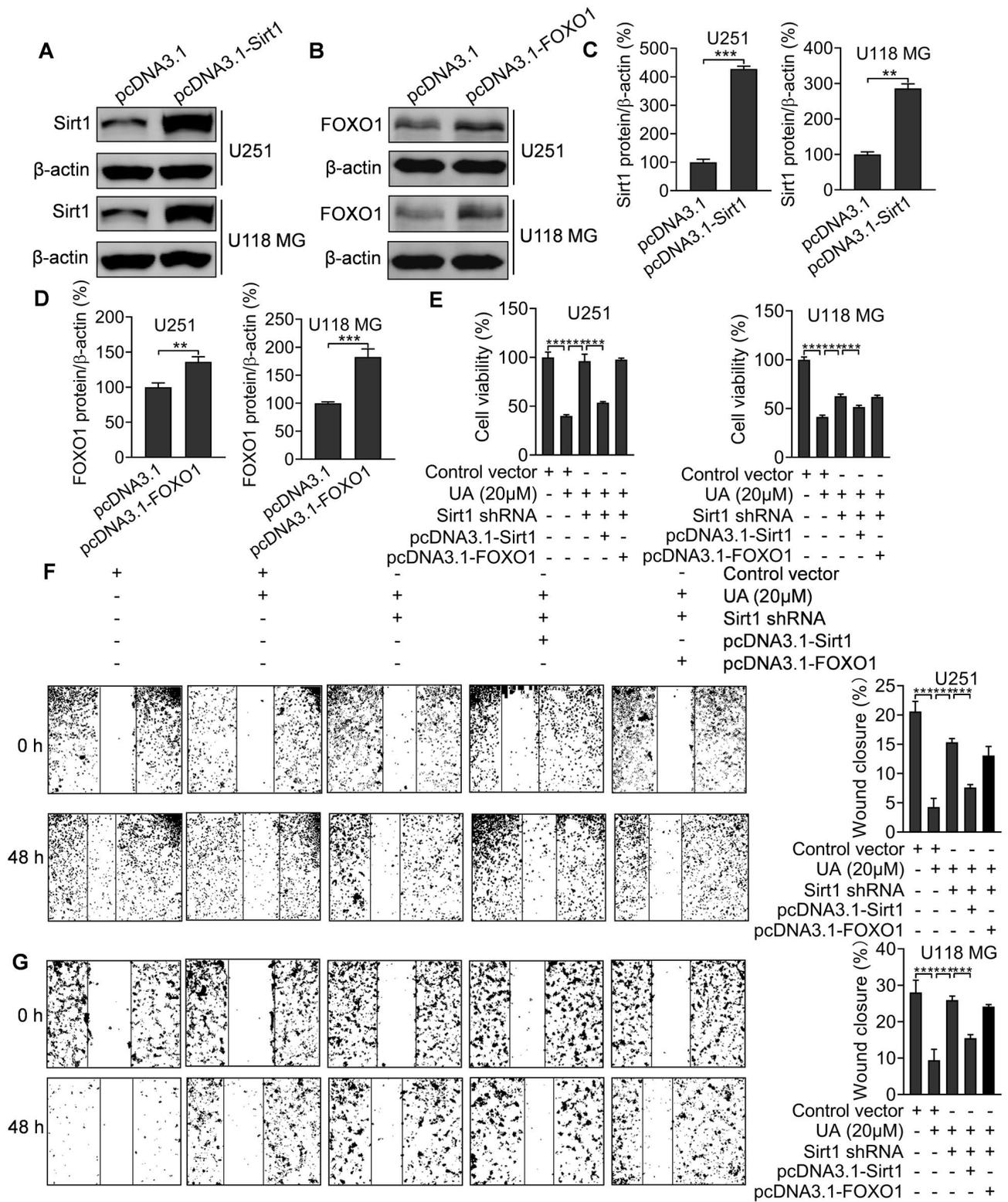
Figure 3. Effect of UA on the cell cycle and apoptosis of glioblastoma cells. A) Quantified analysis of the cell cycle results performed after UA treatment for 24 h. B, C) The mRNA and protein levels of the Cyclin D1 and CDK4 in U251 cells were assessed. D) Quantification analysis of apoptosis ratio indicated that UA induced apoptosis of U251 and U118 MG cells. E) The protein levels of Bcl-2, Bax, and Cytochrome C after UA treatment were assessed by western blotting. F) Quantified analysis of the western blotting. G) The protein levels of Cytochrome C in mitochondria and cytoplasm after UA treatment were assessed by western blotting. n=6; *p<0.05, **p<0.01, ***p<0.01 vs. vehicle-treated group

Figure 4. UA induced the up-regulation of Sirt1 and FOXO1 in U251 cells. A) Survival probability analysis of low and highly expressed Sirt1 in glioblastoma patients from the CGGA database. B) The analysis of the mRNA levels of Sirt1 in glioblastoma tumors of different WHO grades based on the CGGA database. C) The mRNA levels of Sirt1 in glioblastoma and normal human astrocytes. D, E) The mRNA and protein levels of Sirt1 after treatment with UA. F, G) The mRNA and protein levels of FOXO1 after treatment with UA. H) The correlation analysis of mRNA or protein levels between Sirt1 and FOXO1. n=6; *p<0.05, **p<0.01, ***p<0.01 vs. vehicle-treated group

Figure 5. Knockdown of Sirt1 blocked the repressive effect of UA on the proliferation and migration of glioblastoma cells. A) The low protein expression levels of Sirt1 induced by targeted shRNA. B, C) The cells were transferred with Sirt1 shRNA, incubated with UA, and measured for the cell viability and migration measured by CCK-8 and wound-healing assays. D) The protein level of FOXO1 was assessed by western blotting. (Original magnification, 40×). n=6; *p<0.05, **p<0.01, ***p<0.01 vs. vehicle-treated group

Figure 6. The rescued effect of overexpression of Sirt1 or FOXO1 on the dysfunctional effect of UA induced by Sirt1 knockout on the proliferation and migration of glioblastoma cells. A, B) The western blotting showing the expression levels of Sirt1 and FOXO1 induced by targeted overexpression vectors. **C, D)** The quantitative analysis of expression levels. **E–G)** The cells were transferred with Sirt1 shRNA, then Sirt1 or FOXO1 overexpression vector, and incubated with UA, and the cell viability and migration were measured by CCK-8 and wound-healing assays. (Original magnification, 40×). n=6; **p<0.01, ***p<0.01 vs. vehicle-treated group

analysis results indicated that the mRNA or protein levels of Sirt1 were positively correlated with the mRNA or protein levels of FOXO1, respectively (Figure 4H).

Next, we investigated whether Sirt1 mediated the inhibitory effect of UA on proliferation and migration. We synthesized the Sirt1-targeted shRNA, and the validation results revealed that Sirt1-targeted shRNA significantly reduced the protein expression levels of Sirt1 (Figure 5A). Furthermore, our results demonstrated that the knockdown of Sirt1 blocked the inhibitory effect of UA on the proliferation and migration of U251 and U118 MG cells (Figures 5B, 5C). Moreover, the Sirt1 knockdown also blocked the effect of UA on the upregulation of FOXO1 (Figure 5D). In order to further explore the mediatory effects of Sirt1 and FOXO1 on the inhibitory activity of UA in proliferation and migration of U251 and U118 MG cells, we synthesized the Sirt1 or FOXO1-targeted overexpression vector, and the validation results revealed that these vectors significantly increased the Sirt1 or FOXO1 protein expression levels respectively (Figures 6A–6D). Moreover, our results indicated that the overexpression of Sirt1, but not FOXO1 restored the despaired inhibitory effect of UA induced by Sirt1 knockout on the proliferation and migration of U251 and U118 MG cells (Figures 6E–6G).
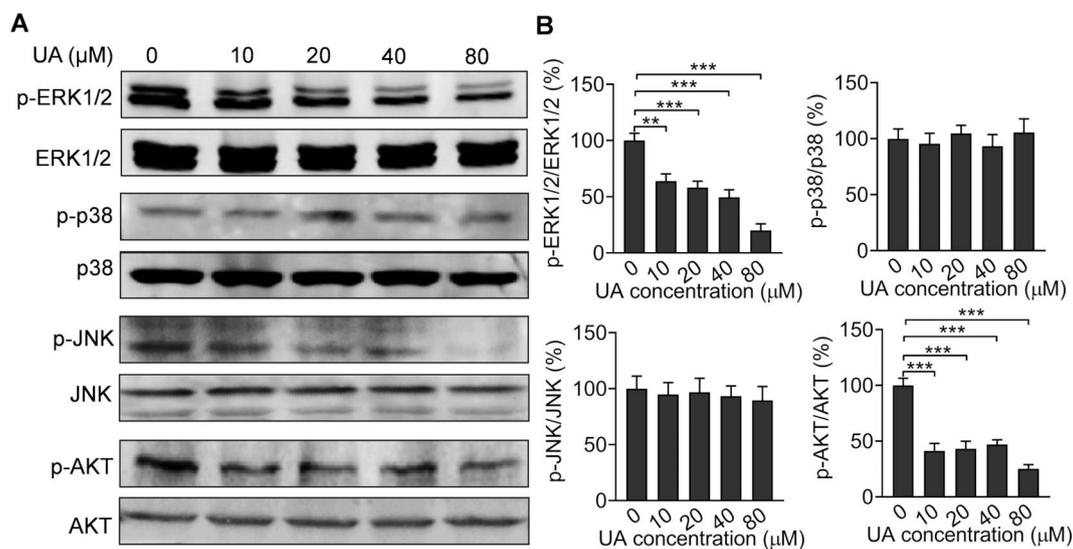
In order to investigate the underlying pathway that mediates the activity of UA, the expression of family members of MAPK and AKT was detected in U251cells by western blotting. Our data showed that UA repressed the phosphorylation levels of ERK and AKT, while having no effect on p38 and JNK (Figures 7A, 7B).

UA inhibits the growth of glioblastoma xenografts in nude mice. We aimed to establish a nude mouse model of GBM xenograft to examine the inhibitory effect of UA on tumor growth *in vivo*. The results indicated that the tumor volume (Figure 8A) and tumor weight (Figures 8B, 8C) were significantly decreased in mice treated with UA for 15 days compared to the control group. Meanwhile, Figure 8D showed that UA apparently reduced the protein expression levels of Sirt1 and FOXO1 in tumor tissues. Meanwhile, the correlation analysis results indicated that the protein levels of Sirt1 in tumor tissues were positively correlated with the protein levels of FOXO1 (Figure 8E). Furthermore, the immunofluorescence staining results also indicated that immunofluorescence signals of Sirt1 and FOXO1 in tumor tissues were increased by UA treatment compared to vehicle treatment (Figures 8F, 8G).

Discussion

In this study, we found that UA significantly inhibited glioblastoma growth, colony formation ability, migration and invasion in a dose- or time-dependent manner. Meanwhile, UA repressed the EMT of U251 cells. Moreover, glioblastoma cell cycle arrest and apoptosis were induced by UA. Furthermore, the expression levels of Sirt1 and FOXO1 were found to increase after UA treatment, and the knockdown of Sirt1 interfered with the inhibitory effects of UA, with the corresponding changes in FOXO1 expression, while, overexpression of Sirt1, but not FOXO1 restored the despaired inhibitory effect of UA induced by Sirt1 knockout on the proliferation and migration of glioblastoma cells. UA also expressed suppressive activity on glioblastoma growth in xenograft nude mouse models, with the opposite regulatory effect on the expression of Sirt1 and FOXO1. Our results indicated that UA inhibits the growth and metastasis of glioblastoma cells by regulating the Sirt1-FOXO1 axis via ERK/AKT signaling pathways (Figure 9).

Figure 7. The expressions of MAPKs and AKT in the U251 cell line with various concentrations of UA treatments. A) The western blotting showing the expression levels of MAPKs and AKT. (B) The quantitative analysis of expression levels of MAPKs and AKT. n=6; **p<0.01, ***p<0.01 vs.vehicle-treated group
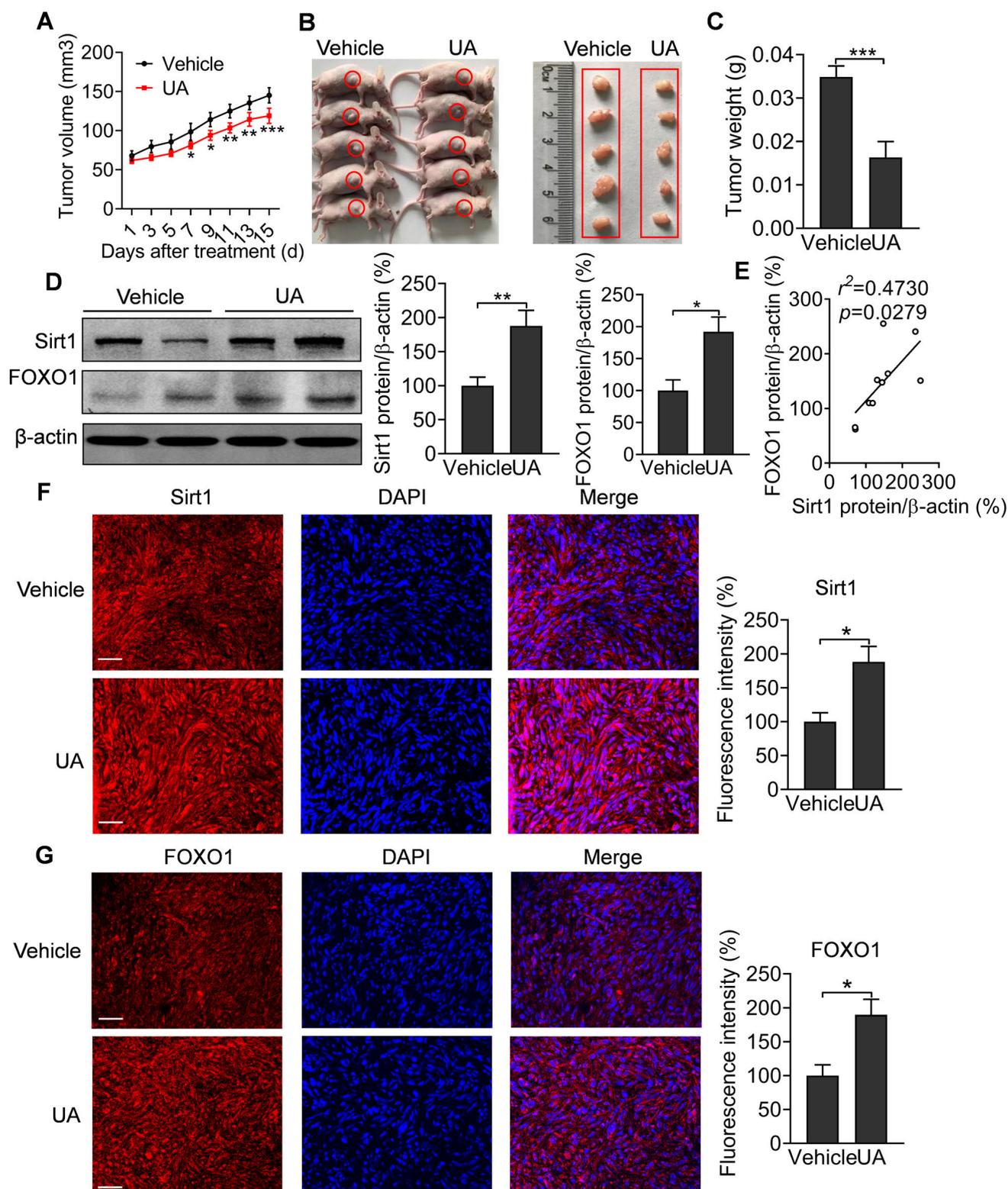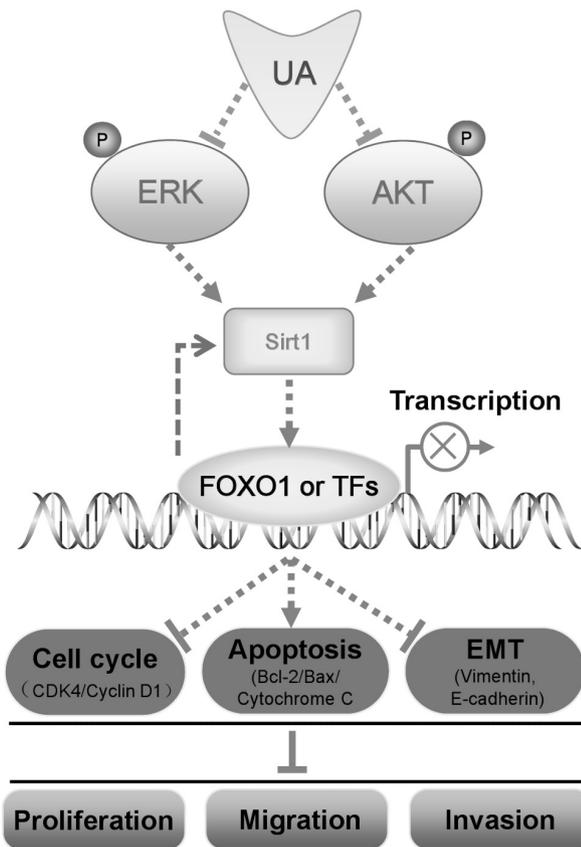
Figure 8. UA inhibited the growth of GMB tumors *in vivo*. The transplant tumor model was built by inoculating U251 cells into nude mice. A) Tumor volumes were calculated every two days. B) The representative image showing the tumor volumes. C) Tumor weight was calculated after harvesting the tumor. D) The protein expression levels of Sirt1 in tumors treated with vehicle or UA. E) The correlation analysis of protein levels between Sirt1 and FOXO1. F, G) Immunofluorescence image and fluorescence intensity analysis showing the Sirt1 or FOXO1 (red)-expressing levels in tumors after vehicle or UA treatment. Nucleus: Blue. Scale bar=50 μm; n=5; **p<0.01, ***p<0.01 vs. vehicle-treated group

Figure 9. Schematic diagram illustrating the mechanism by which UA suppresses glioblastoma progression by regulating Sirt1-FOXO1 axis via ERK/AKT signaling pathways.

Although reports on the expression levels of Sirt1 in glioblastoma have been contradictory [34–36], it was commonly acknowledged that Sirt1 plays a significant role in many cancers [37, 38]. In our research, we found that high levels of Sirt1 expression were associated with a high survival rate in glioblastoma patients. By contrast, Sirt1 expression was downregulated in glioblastoma cells, suggesting that Sirt1 is an antitumor gene for glioblastoma. Moreover, UA increased the expression of Sirt1, and inhibition of Sirt1 expression was found to block the suppressive effect of UA on glioblastoma cells, and overexpression of Sirt1 restored the despaired inhibitory effect of UA induced by Sirt1 knockout, indicating that Sirt1 is indeed the underlying functional target gene of UA. The mechanism for this regulatory process may occur via the modulation of signaling pathways [39, 40]. Our results showed that UA suppressed the activity of ERK and AKT pathways, which may mediate the effect on the transcriptional regulation of targeted genes because it was reported that inhibition of PI3K/AKT and MEK/ERK pathways activates FOXO transcription factors [41, 42], which may result in the enhanced expression of Sirt1. Besides, inhibiting Sirt1 activity or siRNA-mediated Sirt1 knockout

significantly reduces ERK1/2 activation [43], which formed a negative feedback regulation. Nevertheless, the elucidation of the exact pathways involved in the regulatory effect of UA on Sirt1 requires further exploration by using specific inhibitors of certain signaling pathways.

Generally, the functional role of Sirt1 in cancer can be achieved via the deacetylation of histone and non-histone proteins [37]. Numerous studies have reported that FOXO1 acts as a tumor suppressor, inhibiting the development of different types of cancer, where FOXO1 inactivation is accompanied by a poor prognosis in patients [21, 44]. It is interesting to note that UA can induce the upregulation of FOXO1, which is positively correlated with Sirt1, implying that, except for deacetylating modification, the transcription or translation of FOXO1 may be affected by Sirt1. However, we also found that overexpression of FOXO1 cannot rescue the despaired inhibitory effect of UA induced by Sirt1 knockout, indicating that FOXO1 may be not the unique underlying targeted functional gene mediating the activity of UA. Meanwhile, Sirt1 inhibits the transcriptional activity of p53, FOXO3, and E2F1 by directly binding and deacetylating [37, 45, 46]. Furthermore, PGC-1α has been reported to be a critical target of Sirt1 deacetylation activity. The transcriptional activity of PGC-1α is affected by Sirt1 via deacetylation [47], while the acetylation of PGC-1α suppresses its transcriptional activity [48] and the subsequent expression of its target genes. To be confusing, FOXO1 is also a reported transcription factor, which in turn, regulates the expression of Sirt1. Therefore, the exact functional mechanisms need to be elucidated in future studies.

The penetration of BBB is an important limiting factor for the use of chemotherapeutic drugs in the treatment of glioblastoma, since the BBB serves as a physical and physiological barrier for drug delivery to glioblastoma [49]. Therefore, it is conventional for therapies designed for use in the central nervous system to pass through the BBB. Certain studies have shown that UA is able to pass through the BBB [50], with therapeutic evidence of the anti-Alzheimer's disease effects of UA in an animal model when administrated in the periphery [51]. The ability of UA to penetrate BBB makes it a great potential drug for the treatment of glioblastoma.

In conclusion, UA was found to exert an inhibitory effect on the tumor growth and metastasis of glioblastoma, as well as inducing cell cycle and apoptosis in glioblastoma cells. Intriguingly, UA was also found to regulate the Sirt1-FOXO1 axis, and interfering with Sirt1 expression blocked the effects of UA on glioblastoma cells. Furthermore, UA was found to inhibit the growth of glioblastoma in xenograft mice. Our findings provide the research basis for the clinical usage of UA and the evidence for the further exploration of potential antitumor drugs.

Supplementary information is available in the online version of the paper.

References

[1] MCNEILL KA. Epidemiology of brain tumors. Neurol Clin 2016; 34: 981–998. https://doi.org/10.1016/j.ncl.2016.06.014

[2] HANSEN S, RASMUSSEN BK, LAURSEN RJ, KOSTEL-JANETZ M, SCHULTZ H et al. Treatment and survival of glioblastoma patients in denmark: The danish neuro-oncology registry 2009–2014. J Neurooncol 2018; 139: 479–489. https://doi.org/10.1007/s11060-018-2892-7

[3] STUPP RWEBER DC. The role of radio- and chemotherapy in glioblastoma. Onkologie 2005; 28: 315–317. https://doi.org/10.1159/000085575

[4] DOTTO GP. Crosstalk of notch with p53 and p63 in cancer growth control. Nat Rev Cancer 2009; 9: 587–595. https://doi.org/10.1038/nrc2675

[5] SCHERNBERG A, MARABELLE A, MASSARD C, ARMAND JP, DUMONT S et al. [what's next in glioblastoma treatment: Tumor-targeted or immune-targeted therapies?]. Bull Cancer 2016; 103: 484–498. https://doi.org/10.1016/j.bulcan.2016.02.014

[6] ESPIN JC, LARROSA M, GARCIA-CONESA MTTOMAS-BARBERAN F. Biological significance of urolithins, the gut microbial ellagic acid-derived metabolites: The evidence so far. Evid Based Complement Alternat Med 2013; 2013: 270418. https://doi.org/10.1155/2013/270418

[7] BAKKALBASI E, MENTES OARTIK N. Food ellagitannins-occurrence, effects of processing and storage. Crit Rev Food Sci Nutr 2009; 49: 283–298. https://doi.org/10.1080/10408390802064404

[8] RYU D, MOUCHIROUD L, ANDREUX PA, KATSYUBA E, MOULLAN N et al. Urolithin a induces mitophagy and prolongs lifespan in c. Elegans and increases muscle function in rodents. Nat Med 2016; 22: 879–888. https://doi.org/10.1038/nm.4132

[9] LIPINSKA L, KLEWICKA ESOJKA M. The structure, occurrence and biological activity of ellagitannins: A general review. Acta Sci Pol Technol Aliment 2014; 13: 289–299. https://doi.org/10.17306/j.afs.2014.3.7

[10] SANCHEZ-GONZALEZ C, CIUDAD CJ, IZQUIERDO-PULIDO MNOE V. Urolithin a causes p21 up-regulation in prostate cancer cells. Eur J Nutr 2016; 55: 1099–1112. https://doi.org/10.1007/s00394-015-0924-z

[11] GOSSAGE LEISEN T. Targeting multiple kinase pathways: A change in paradigm. Clin Cancer Res 2010; 16: 1973–1978. https://doi.org/10.1158/1078-0432.CCR-09-3182

[12] TOMAS-BARBERAN FA, GONZALEZ-SARRIAS A, GARCIA-VILLALBA R, NUNEZ-SANCHEZ MA, SELMA MV et al. Urolithins, the rescue of "old" metabolites to understand a "new" concept: Metabotypes as a nexus among phenolic metabolism, microbiota dysbiosis, and host health status. Mol Nutr Food Res 2017; 61: https://doi.org/10.1002/mnfr.201500901

[13] HAIGIS MCSINCLAIR DA. Mammalian sirtuins: Biological insights and disease relevance. Annu Rev Pathol 2010; 5: 253–295. https://doi.org/10.1146/annurev.pathol.4.110807.092250

[14] BOSCH-PRESEGUE LVAQUERO A. Sirtuin-dependent epigenetic regulation in the maintenance of genome integrity. FEBS J 2015; 282: 1745–1767. https://doi.org/10.1111/febs.13053

[15] VAZIRI H, DESSAIN SK, NG EATON E, IMAI SI, FRYE RA et al. Hsir2(sirt1) functions as an nad-dependent p53 deacetylase. Cell 2001; 107: 149–159. https://doi.org/10.1016/s0092-8674(01)00527-x

[16] HALLOWS WC, YU WDENU JM. Regulation of glycolytic enzyme phosphoglycerate mutase-1 by sirt1 protein-mediated deacetylation. J Biol Chem 2012; 287: 3850–3858. https://doi.org/10.1074/jbc.M111.317404

[17] PURUSHOTHAM A, XU QLI X. Systemic sirt1 insufficiency results in disruption of energy homeostasis and steroid hormone metabolism upon high-fat-diet feeding. FASEB J 2012; 26: 656–667. https://doi.org/10.1096/fj.11-195172

[18] PENG L, YUAN Z, LING H, FUKASAWA K, ROBERTSON K et al. Sirt1 deacetylates the DNA methyltransferase 1 (dnmt1) protein and alters its activities. Mol Cell Biol 2011; 31: 4720–4734. https://doi.org/10.1128/MCB.06147-11

[19] FIRESTEIN R, BLANDER G, MICHAN S, OBERDOERFFER P, OGINO S et al. The sirt1 deacetylase suppresses intestinal tumorigenesis and colon cancer growth. PLoS One 2008; 3: e2020. https://doi.org/10.1371/journal.pone.0002020

[20] ZANELLA F, LINK WCARNERO A. Understanding foxo, new views on old transcription factors. Curr Cancer Drug Targets 2010; 10: 135–146. https://doi.org/10.2174/156800910791054158

[21] SONG HM, SONG JL, LI DF, HUA KY, ZHAO BK et al. Inhibition of foxo1 by small interfering rna enhances proliferation and inhibits apoptosis of papillary thyroid carcinoma cells via akt/foxo1/bim pathway. Onco Targets Ther 2015; 8: 3565–3573. https://doi.org/10.2147/OTT.S95395

[22] CHENG C, JIAO JT, QIAN Y, GUO XY, HUANG J et al. Curcumin induces g2/m arrest and triggers apoptosis via foxo1 signaling in u87 human glioma cells. Mol Med Rep 2016; 13: 3763–3770. https://doi.org/10.3892/mmr.2016.5037

[23] LI C, MENG F, GARZA JC, LIU J, LEI Y et al. Modulation of depression-related behaviors by adiponectin adipor1 receptors in 5-ht neurons. Mol Psychiatry 2020; https://doi.org/10.1038/s41380-020-0649-0

[24] MENG F, LIU J, DAI J, WU M, WANG W et al. Brain-derived neurotrophic factor in 5-ht neurons regulates susceptibility to depression-related behaviors induced by subchronic unpredictable stress. J Psychiatr Res 2020; 126: 55–66. https://doi.org/10.1016/j.jpsychires.2020.05.003

[25] LIU J, MENG F, DAI J, WU M, WANG W et al. The bdnf-foxo1 axis in the medial prefrontal cortex modulates depressive-like behaviors induced by chronic unpredictable stress in postpartum female mice. Mol Brain 2020; 13: 91. https://doi.org/10.1186/s13041-020-00631-3

[26] LIVAK KJSCHMITTGEN TD. Analysis of relative gene expression data using real-time quantitative pcr and the 2− δδct method. methods 2001; 25: 402–408. https://doi.org/10.1006/meth.2001.1262

[27] LI C, MENG F, LEI Y, LIU J, LIU J et al. Leptin regulates exon-specific transcription of the bdnf gene via epigenetic modifications mediated by an akt/p300 hat cascade. Mol Psychiatry 2020; https://doi.org/10.1038/s41380-020-00922-0

[28] CHEN W, AN J, GUO J, WU Y, YANG L et al. Sodium selenite attenuates lung adenocarcinoma progression by repressing sox2-mediated stemness. Cancer Chemother Pharmacol 2018; 81: 885–895. https://doi.org/10.1007/s00280-018-3561-4

[29] XING JS, WANG X, LAN YL, LOU JC, MA B et al. Isoalantolactone inhibits ikkbeta kinase activity to interrupt the nf-kappab/cox-2-mediated signaling cascade and induces apoptosis regulated by the mitochondrial translocation of cofilin in glioblastoma. Cancer Med 2019; 8: 1655–1670. https://doi.org/10.1002/cam4.2013

[30] MIYAI M, TOMITA H, SOEDA A, YANO H, IWAMA T et al. Current trends in mouse models of glioblastoma. J Neurooncol 2017; 135: 423–432. https://doi.org/10.1007/s11060-017-2626-2

[31] DEBATIN KM. Apoptosis pathways in cancer and cancer therapy. Cancer Immunol Immunother 2004; 53: 153–159. https://doi.org/10.1007/s00262-003-0474-8

[32] MUNEESWARAN G, KARTHEESWARAN S, MUTHU-KUMAR KKARUNAKARAN C. Temperature-dependent conformational dynamics of cytochrome c: Implications in apoptosis. J Mol Graph Model 2018; 79: 140–148. https://doi.org/10.1016/j.jmgm.2017.10.008

[33] OTT M, ROBERTSON JD, GOGVADZE V, ZHIVOTOVSKY BORRENIUS S. Cytochrome c release from mitochondria proceeds by a two-step process. Proc Natl Acad Sci U S A 2002; 99: 1259–1263. https://doi.org/10.1073/pnas.241655498

[34] LAI SW, LIU YS, LU DYTSAI CF. Melatonin modulates the microenvironment of glioblastoma multiforme by targeting sirtuin 1. Nutrients 2019; 11: https://doi.org/10.3390/nu11061343

[35] FANG DZ, WANG WJ, LI FY, LIU J, HUI XB et al. Circ_0005075 stimulates the proliferation and metastasis of glioma via downregulating sirt1. Eur Rev Med Pharmacol Sci 2020; 24: 258–266. https://doi.org/10.26355/eurrev_202001_19918

[36] CHEN H, LU Q, FEI X, SHEN L, JIANG D et al. Mir-22 inhibits the proliferation, motility, and invasion of human glioblastoma cells by directly targeting sirt1. Tumour Biol 2016; 37: 6761–6768. https://doi.org/10.1007/s13277-015-4575-8

[37] LIU T, LIU PYMARSHALL GM. The critical role of the class iii histone deacetylase sirt1 in cancer. Cancer Res 2009; 69: 1702–1705. https://doi.org/10.1158/0008-5472.CAN-08-3365

[38] DONG G, WANG B, AN Y, LI J, WANG X et al. Sirt1 suppresses the migration and invasion of gastric cancer by regulating arhgap5 expression. Cell Death Dis 2018; 9: 977. https://doi.org/10.1038/s41419-018-1033-8

[39] TOTIGER TM, SRINIVASAN S, JALA VR, LAMICHHANE P, DOSCH AR et al. Urolithin a, a novel natural compound to target pi3k/akt/mtor pathway in pancreatic cancer. Mol Cancer Ther 2019; 18: 301–311. https://doi.org/10.1158/1535-7163.MCT-18-0464

[40] HAN QA, YAN C, WANG L, LI G, XU Y et al. Urolithin a attenuates ox-ldl-induced endothelial dysfunction partly by modulating microrna-27 and erk/ppar-gamma pathway. Mol Nutr Food Res 2016; 60: 1933–1943. https://doi.org/10.1002/mnfr.201500827

[41] ROY SK, SRIVASTAVA RKSHANKAR S. Inhibition of pi3k/akt and mapk/erk pathways causes activation of foxo transcription factor, leading to cell cycle arrest and apoptosis in pancreatic cancer. J Mol Signal 2010; 5: 10. https://doi.org/10.1186/1750-2187-5-10

[42] SHANKAR S, CHEN QSRIVASTAVA RK. Inhibition of pi3k/akt and mek/erk pathways act synergistically to enhance antiangiogenic effects of egcg through activation of foxo transcription factor. J Mol Signal 2008; 3: 7. https://doi.org/10.1186/1750-2187-3-7

[43] ZHAO Y, LUO P, GUO Q, LI S, ZHANG L et al. Interactions between sirt1 and mapk/erk regulate neuronal apoptosis induced by traumatic brain injury in vitro and in vivo. Exp Neurol 2012; 237: 489–498. https://doi.org/10.1016/j.expneurol.2012.07.004

[44] COOMANS DE BRACHENE ADEMOULIN JB. Foxo transcription factors in cancer development and therapy. Cell Mol Life Sci 2016; 73: 1159–1172. https://doi.org/10.1007/s00018-015-2112-y

[45] WANG C, CHEN L, HOU X, LI Z, KABRA N et al. Interactions between e2f1 and sirt1 regulate apoptotic response to DNA damage. Nat Cell Biol 2006; 8: 1025–1031. https://doi.org/10.1038/ncb1468

[46] HELTWEG B, GATBONTON T, SCHULER AD, POSAKONY J, LI H et al. Antitumor activity of a small-molecule inhibitor of human silent information regulator 2 enzymes. Cancer Res 2006; 66: 4368–4377. https://doi.org/10.1158/0008-5472.CAN-05-3617

[47] RODGERS JT, LERIN C, HAAS W, GYGI SP, SPIEGELMAN BM et al. Nutrient control of glucose homeostasis through a complex of pgc-1alpha and sirt1. Nature 2005; 434: 113–118. https://doi.org/10.1038/nature03354

[48] LERIN C, RODGERS JT, KALUME DE, KIM SH, PANDEY A et al. Gcn5 acetyltransferase complex controls glucose metabolism through transcriptional repression of pgc-1alpha. Cell Metab 2006; 3: 429–438. https://doi.org/10.1016/j.cmet.2006.04.013

[49] DREAN A, GOLDWIRT L, VERREAULT M, CANNEY M, SCHMITT C et al. Blood-brain barrier, cytotoxic chemotherapies and glioblastoma. Expert Rev Neurother 2016; 16: 1285–1300. https://doi.org/10.1080/14737175.2016.1202761

[50] YUAN T, MA H, LIU W, NIESEN DB, SHAH N et al. Pomegranate's neuroprotective effects against alzheimer's disease are mediated by urolithins, its ellagitannin-gut microbial derived metabolites. ACS Chem Neurosci 2016; 7: 26–33. https://doi.org/10.1021/acschemneuro.5b00260

[51] GONG Z, HUANG J, XU B, OU Z, ZHANG L et al. Urolithin a attenuates memory impairment and neuroinflammation in app/ps1 mice. J Neuroinflammation 2019; 16: 62. https://doi.org/10.1186/s12974-019-1450-3